# Phosphogluconolactonase as the linchpin of an efficient pentose phosphate pathway

Léa Phégnon[1‡], Julien Pérochon[1‡], Sandrine Uttenweiler-Joseph[1], Edern Cahoreau[1,2], Pierre Millard[1,2] and Fabien Létisse[1,3*]

[1]Toulouse Biotechnology Institute, Université de Toulouse, INSA, UPS, Toulouse, France.

[2]MetaToul-MetaboHUB, National Infrastructure of Metabolomics and Fluxomics, Toulouse, France.

[3]Institut de Pharmacologie et de Biologie Structurale (IPBS), Université de Toulouse, CNRS, Université Toulouse III - Paul Sabatier (UT3), Toulouse, France

***Corresponding author**

Fabien Létisse: fabien.letisse@univ-tlse3.fr

[‡]Co first authors

15 **ABBREVIATIONS:**

16 6PGL : 6-Phosphogluconolactone

17 δ-6PGL : δ-6-phosphogluconolactone

18 GNT: Gluconate

19 6PGNT: 6-phosphogluconate

20 oxPPP: oxidative branch of the pentose-phosphate pathway

21

22

23

**ABSTRACT:**

The metabolic networks of microorganisms are remarkably robust to genetic and environmental perturbations. This robustness stems from redundancies such as gene duplications, isoenzymes, alternative metabolic pathways, and also from non-enzymatic reactions. In the oxidative branch of the pentose-phosphate pathway (oxPPP), 6-phosphogluconolactone hydrolysis into 6-phosphogluconate is catalysed by 6-phosphogluconolactonase (Pgl) but in the absence of the latter, the oxPPP flux is thought to be maintained by spontaneous hydrolysis. However, in Δ*pgl Escherichia coli*, an extracellular pathway can also contribute to pentose-phosphate synthesis. This raises question as to whether the non-enzymatic reaction can compensate for the absence of 6-phosphogluconolactonase and, ultimately, on the role of 6-phosphogluconolactonase in central metabolism. Our results indicate that in the absence of Pgl, this bypass pathway accounts for the entire flux into the oxPPP, suggesting that non-enzymatic hydrolysis does not compensate for the absence of Pgl and demonstrating that Pgl is critical for an efficiently functioning oxPPP.

38 **INTRODUCTION**

39 Metabolic networks are a set of interconnected chemical reactions, most of which are catalysed by
40 enzymes. The interplay between chemical reactions provides alternative routes for adaptation to
41 genetic or environmental perturbations; the network organisation of metabolic systems thus
42 underpins the metabolic robustness and adaptability of cells. The central metabolism of *Escherichia*
43 *coli* is a model of metabolic robustness since very few of the associated genes are indispensable for
44 growth on glucose minimal medium[1,2]. Furthermore, *E. coli* knock-out mutants lacking key central
45 metabolic enzymes have similar growth phenotypes[3–7]. This robustness is in part the result of
46 metabolic flux rerouting[6,7] but stems also from local compensatory mechanisms based on redundancy,
47 such as the presence of isozymes and alternative pathways[2–5,7].

48 Compensatory mechanisms involving non-enzymatic reactions are harder to identify because they
49 cannot be studied by metabolic reconstruction using comparative genomics[8]. These mechanisms are
50 based on specific or non-specific chemical reactions that occur either exclusively non-enzymatically
51 within the metabolic network, or in parallel to existing enzyme functions[9]. The second step in the
52 oxidative branch of the pentose-phosphate pathway (oxPPP), the spontaneous hydrolysis of δ-6-
53 phosphogluconolactone (δ-6PGL) into 6-phosphogluconate (6PGNT) is an archetypal example of a
54 reaction that can occur enzymatically, catalysed by 6-phosphogluconolactonase (Pgl, EC 3.1.1.31), and
55 non-enzymatically, without Pgl activity. However, Pgl's main role, rather than maintaining the flux
56 through the PPP, is thought to be preventing the formation of unwanted side-products by covalent
57 modification with highly reactive 6PGLs (δ (1-5) and γ (1-4))[10–12]. In pioneering studies, Kupor and
58 Fraenkel[13,14] found that absence of the *pgl* gene indeed slowed the growth of *E. coli* on glucose, but
59 more importantly perhaps, they also discovered an alternative pathway bypassing Pgl, involving
60 dephosphorylation and secretion of gluconolactone, spontaneous abiotic hydrolysis in the medium,
61 and re-import of gluconate and phosphorylation[14]. This "Pgl bypass" can therefore provide the same
62 anabolic precursors (NADPH and pentose-phosphates) as the canonical oxPPP.

63 In *E. coli*, one fifth of glucose uptake is directed towards the oxPPP to provide the required anabolic
64 precursors[6], highlighting the importance of this pathway. In the absence of Pgl, it is thought that this
65 flux is maintained by rapid non-enzymatic hydrolysis of δ-6PGL rather than by the Pgl bypass[7,11,14,15].
66 However, 6PGLs have a non-negligible lifetime[11], raising the questions whether spontaneous δ-6PGL
67 hydrolysis is fast enough to maintain a high flux through the oxPPP in the absence of Pgl and how the
68 bypass pathway might contribute.

69 In this study, we used a metabolic flux approach to investigate *E. coli* oxPPP function in the absence of
70 Pgl to (i) reinvestigate the extracellular bypass pathway identified by Kupor and Fraenkel using state-
71 of-the-art methods, (ii) quantify its contribution to oxPPP flux, and (iii) elucidate the metabolic function
72 of Pgl. In the absence of Pgl, we found that virtually all carbon flux through the oxPPP was channelled
73 through the Pgl bypass, and that the contribution of non-enzymatic δ-6PGL hydrolysis was negligible.
74 This in turn suggests that the catalytic function of Pgl is required to maintain high flux through the
75 canonical oxPPP, and that the metabolic role of this enzyme is more substantial than simple house-
76 cleaning duties.

77

78 **RESULTS**

79 **Slow growth in *E. coli* Δ*pgl* is accompanied by gluconate accumulation in the culture medium**

80 We first sought to determine the growth phenotype of an *E. coli* K-12 strain lacking *pgl*, grown on
81 minimal medium with glucose (15 mM) as sole carbon source (Table 1 and supplementary 1 figure 1).
82 In agreement with Kupor and Fraenkel's[14] findings, the Δ*pgl* strain grew much slower than the WT. The
83 specific rate of acetate production was markedly increased in the Δ*pgl* strain, resulting in a higher
84 acetate yield (0.54 ± 0.03 mol/mol) than in the WT strain (0.31 ± 0.02 mol/mol), as observed
85 previously[7]. In addition to acetate and other metabolites previously detected by $^{1}$H NMR[16], significant
86 amounts of gluconate were also detected, but only in the culture medium of the Δ*pgl* strain (Table 1
87 and supplementary 1 figure 2). Gluconate accumulation represented approximately 2% of the total
88 carbon flux entering the central metabolic pathways of the *Δpgl* strain (Table 1). Note that no 6PGL
89 was detected in the culture supernatant of the *Δpgl* strain (Supplementary 1 figure 2).
90 Complementation of the Δ*pgl* strain with the WT gene restored the growth rate determined for the
91 WT *E. coli*, without any gluconate accumulation (Table 1), demonstrating that reduced growth and
92 gluconate excretion are related to the absence of Pgl.

93 **Gluconate is formed by abiotic degradation of gluconolactone**

94 In the extracellular Pgl bypass proposed by Kupor and Fraenkel[14], gluconolactones are hydrolysed into
95 gluconate abiotically in the culture medium. The obvious explanation for the presence of gluconate in
96 the extracellular medium is therefore that gluconolactones are fully converted into gluconate within
97 the time taken to sample the culture medium and store the samples. To prevent abiotic hydrolysis, the
98 culture medium was sampled by filtration, placed immediately on ice and then analysed by NMR, with
99 the first spectrum recorded approximately 5 min after sample withdrawal. Both isomeric forms of
100 gluconolactone (δ and γ) were detected in equal amounts whereas the gluconate concentration was
101 below the detection limit (Supplementary 1 figure 3). 6PGL was not detected either. Importantly, the
102 total amount of gluconolactones was similar to the amount of gluconate detected in the corresponding

103 sample obtained with the initial procedure, indicating that rapidly reducing the sample temperature
104 prevents the spontaneous degradation of gluconolactones. To confirm this effect, we measured the
105 rate constants of gluconolactone spontaneous non-enzymatic hydrolysis in fresh minimal medium
106 containing commercial gluconolactone using real-time $^{1}$H-NMR (Figure 1). The degradation constants
107 obtained by fitting the gluconolactone concentration–time curves assuming a first-order process[17]
108 were $0.36 \pm 0.01$ h$^{-1}$ at 7 °C and $2.58 \pm 0.02$ h$^{-1}$ at 37 °C. At 7 °C therefore, the amount of gluconolactone
109 hydrolysed during 5 min of sample preparation is negligible. Using the same approach, the hydrolysis
110 rate of δ-6PGL was found to be $3.97 \pm 0.04$ h$^{-1}$ at 37 °C, about 6-7 times higher than at 5°C[11]
111 (Supplementary 1 figure 4) and the same order of magnitude as measured for gluconolactone.

112 The detection of gluconate in the culture medium in the above experiments is therefore an
113 experimental artefact arising from the hydrolysis of gluconolactones during the sampling process. The
114 Δ*pgl* strain produces gluconolactone (not gluconate) during growth on glucose.

115 **Glucose-derived gluconate is metabolized by canonical gluconate metabolism**

116 Under growth conditions at 37°C, gluconolactones in the culture medium spontaneously hydrolyse to
117 gluconate. However, gluconate remained below the limit of detection when the culture medium was
118 sampled by filtration and rapidly cooled. We therefore hypothesized that the cells consumed gluconate
119 faster than the rate of production by spontaneous hydrolysis. To confirm this, we blocked gluconate
120 utilization by knocking out the two gluconokinases, GntK and IdnK, known to activate gluconate after
121 uptake[18,19]. As reported previously[20], the Δ*gntK* Δ*idnK* double mutant did not grow on D-gluconate as
122 sole carbon source. As expected therefore, gluconate accumulation was observed when the
123 *ΔpglΔgntKΔidnK* triple mutant was grown on glucose, with a specific secretion rate of 1.13 ± 0.04
124 mmol.($g_{CDW}$·h)$^{-1}$. These results are consistent with the Pgl bypass topology described by Kupor and
125 Fraenkel[14] (Figure 2).

126 An unforeseen consequence of gluconokinase deletion was that the Δ*pgl*Δ*gntK*Δ*idnK* triple mutant
127 had a much slower growth rate than the Δ*pgl* strain (0.29 ± 0.01 h$^{-1}$ *vs.* 0.43 ± 0.01 h$^{-1}$). This highlights

128 the importance of metabolic activity in the bypass pathway to sustain growth. To investigate this
129 further, we quantified the metabolic flux through the extracellular bypass using $^{13}C$ metabolic flux
130 analysis. Since the bypass pathway and the non-enzymatic hydrolysis of δ-6PGL operate in parallel
131 without carbon scrambling, their relative contributions to the oxPPP flux cannot be determined using
132 stationary $^{13}C$ labelled experiments alone. We therefore investigated the contributions of both routes
133 in the Δ*pgl* strain using stationary and non-stationary metabolic flux analyses.

134 **Deletion of *pgl* barely modifies the contribution of the oxidative branch of the PPP to glucose**
135 **metabolism**

136 We first quantified the distribution of glucose-6-phosphate between the Embden-Meyerhof-Parnas
137 (EMP) pathway and the oxPPP in the Δ*pgl* strain and the WT strain (as control) grown on minimal M9
138 medium supplemented with [1-$^{13}C$]-glucose as sole carbon source. Metabolic fluxes were inferred from
139 quantitative measurements of $^{13}C$ incorporation into alanine *via* pyruvate (Figure 3). In keeping with
140 previous results[6,21], 17 ± 1 % of glucose was channelled through the oxPPP in the WT strain. In the Δ*pgl*
141 strain, the oxPPP accounted for 15 ± 1 % of glucose uptake, a similar contribution as in the WT strain.
142 This suggests that the absence of Pgl does not lead to a rewiring of central metabolic fluxes, in contrast
143 to what has been observed in the absence of glucose-6-phosphate dehydrogenase, the first enzyme in
144 the oxPPP[6,7]. In the *Δpgl* strain, the metabolic flux through the oxPPP must therefore be maintained by
145 the Pgl bypass and/or by non-enzymatic intracellular hydrolysis of δ-6PGL.

146 **In the absence of Pgl, oxPPP flux passes exclusively though the Pgl bypass**

147 To quantify the contributions of the extracellular bypass and of intracellular non-enzymatic δ-6PGL
148 hydrolysis to oxPPP flux, we performed a non-stationary carbon labelling experiment wherein $^{13}C$
149 labelled glucose was added at the mid-exponential phase to *E. coli* Δ*pgl* growing on unlabelled glucose
150 (Figure 4a and 4c). We used [2-$^{13}C$]-glucose because the NMR signals corresponding to [2-$^{13}C$]-glucose
151 and [2-$^{13}C$]-gluconolactones formed from [2-$^{13}C$]-glucose, are well resolved in 1D,$^{1}H$ NMR spectra,
152 allowing accurate quantification of the total concentrations of unlabelled and labelled gluconolactone

153 (Figure 4b) over time, sampling the culture medium every 30 min after $^{13}C$ labelled glucose was added.
154 Metabolic fluxes were calculated using a differential equation model of the metabolic network shown
155 in Figure 4d. The flux through the oxPPP and the constant rate of gluconolactone hydrolysis were set
156 to their experimentally determined values (Figure 1d and 3c). The metabolic fluxes were then obtained
157 by fitting the time-course concentrations of biomass, (unlabelled and labelled) glucose and (total and
158 $^{13}C$-labelled) gluconolactone. Sensitivity analysis confirmed that the system was identifiable based on
159 the available data, meaning that all fluxes were determined with high precision (relative standard
160 deviation below 5 % in each of the three independent biological replicates).

161 The estimated glucose uptake rates and the growth rates were consistent with data obtained from
162 unlabelled experiments (Table 1). The intracellular branch accounts for a negligible proportion of
163 oxPPP flux (< 1 ± 1 % of glucose uptake), which is fully channelled through the extracellular bypass (99
164 ± 1 %). The bypass carries a flux of 1.07 ± 0.08 mmol·$(g_{CDW}\cdot h)^{-1}$ which is similar to the flux through the
165 canonical oxPPP in the WT strain and much higher than the gluconolactone accumulation flux in
166 unlabelled experiments (0.17 mmol·$(g_{CDW}.h)^{-1}$, Table 1). This flux value is also consistent with the
167 specific gluconate accumulation rate measured in the Δ*pgl*Δ*gntK*Δ*idnK* triple mutant (1.13 ± 0.04
168 mmol·$(g_{CDW}\cdot h)^{-1}$). Overall, these results demonstrate the absence of intracellular flux through the
169 canonical oxPPP under these circumstances, and reveal the key contribution of the extracellular Pgl
170 bypass to R5P biosynthesis in the Δ*pgl* strain. These results also explain the severe growth restriction
171 observed when the Pgl bypass is blocked by the deletion of gluconokinases.

172 **DISCUSSION**

173 To our knowledge this work is the first time the metabolic activity of the Pgl bypass has been
174 quantified, despite its discovery in *E. coli* more than fifty years ago[14]. Our NMR results confirm the
175 bypass topology proposed by Kupor and Fraenkel, although the 6PGL dephosphorylation and (P-
176 )gluconolactone secretion steps remain to be elucidated. Metabolite phosphatases are generally
177 cytosolic, although some have been shown to be periplasmic, notably those involved in nucleotide

178 salvage[22]. If 6PGL is secreted in its phosphorylated form, it should be found in the culture medium
179 based on the spontaneous hydrolysis rate estimated in this work. Since 6PGL was not detected, this
180 suggests it is dephosphorylated intracellularly and that it is the resulting gluconolactone that is then
181 secreted. Nevertheless, further studies are required to identify the genes involved in
182 dephosphorylation and secretion of gluconolactones and to unequivocally resolve the first two steps
183 of the Pgl bypass.

184 Because of this bypass, absence of Pgl leads to substantial gluconolactone excretion – about 17% of
185 the total carbon flux entering the cell. This process, which resembles directed overflow mechanism[23],
186 prevents 6PGL intracellular accumulation, avoiding covalent modifications of proteins[24] and other
187 nucleophiles[10] in the presence of these highly reactive electrophiles. Gluconolactone excretion may
188 therefore be a cleansing mechanism that avoids the formation of toxic metabolites, the function
189 generally ascribed to Pgl[12]. The Pgl bypass may therefore have arisen fortuitously because the unstable
190 gluconolactones excreted into the environment spontaneously hydrolyse into gluconate, one of *E.*
191 *coli*'s preferred carbon sources[25].

192 The Pgl bypass produces pentose-phosphates and NAPDH from G6P with the same stoichiometry as
193 the canonical oxPPP. However, this extracellular metabolic route has a significant energetic cost for
194 the cell. First, one extra mole of ATP is required for the phosphorylation of gluconate by gluconokinases
195 (GntK and IdnK). Second, gluconate import is mediated by proton symport systems driven by the
196 proton motive force (with a stoichiometry of one proton per gluconate[26,27]), thereby consuming
197 protons that could otherwise be used by ATP synthases for ATP production. Assuming a maximal
198 $H^+$/ATP ratio of 4[28], the total energetic cost of the Pgl bypass is 1.25 ATP equivalents per molecule of
199 glucose entering the oxPPP, corresponding to an extra ATP demand of 1.33 mmol·$[g_{CDW} \cdot h]^{-1}$. In other
200 words, roughly 20% of the energy used by the cell for glucose uptake and subsequent phosphorylation
201 by the PTS system is wasted in the Pgl bypass. Furthermore, because gluconolactone hydrolysis occurs
202 non-enzymatically outside the cell, it escapes direct metabolic control and the gluconolactone and

203 gluconate are potentially accessible to other cells competing for carbon sources. An illustrative
204 example of this kind of cross-feeding is the recovery of normal growth in Δ*zwf*Δ*pgi E. coli* in the
205 presence of Δ*pgl* mutants, likely because the gluconolactone or gluconate released by the latter feed
206 the oxPPP of the Δ*zwf*Δ*pgi* cells[15]. The downsides of this extracellular bypass are therefore that it is
207 more energetically expensive, partially beyond metabolic regulation and subject to hijack by
208 competing cells.

209 Two oxPPP topologies must therefore be considered in metabolic flux analyses depending on whether
210 Pgl is present (the canonical oxPPP) or absent (with Pgl bypass). The latter configuration is generally
211 ignored however[7,29], particularly in analyses of *E. coli* BL21[30,31], which is widely used in biotechnological
212 applications, notably for heterologous protein production[32]. *E. coli* BL21 and derived strains lack the
213 *pgl* gene and there is evidence of Pgl bypass activity in this strain[33].

214 Our results show that metabolic activity in the Pgl bypass oxPPP is similar to that of the canonical oxPPP
215 in the WT strain. As observed previously though[7,14,15], the Δ*pgl* mutant grows about 30% slower than
216 the WT. The growth rate is reduced even further if gluconate utilisation is also blocked (down to about
217 50% of the WT's growth rate), highlighting the metabolic contribution of the Pgl bypass. Finally, of the
218 three enzymes involved in the oxPPP (Pgl, G6P dehydrogenase, and 6PGNT dehydrogenase, the latter
219 two being encoded by *zwf* and *gnd* respectively), Pgl is the only one whose absence is associated with
220 a noticeable growth defect. In particular, the silent growth phenotype of the Δ*zwf* mutant
221 demonstrates that flux in the oxPPP is not absolutely required for bacterial growth on glucose. Deletion
222 of *zwf* leads to a global reorganization of metabolic fluxes through *E. coli*'s central metabolism to
223 compensate for the absence of flux in the oxPPP while providing the required precursors and energy
224 for anabolism[6,34,35]. In contrast, *pgl* deletion leads to a local rearrangement of carbon fluxes that fails
225 to support optimal growth. Furthermore, in spite of the secretion mechanism described in this study,
226 absence of Pgl must nevertheless lead to intracellular accumulation of δ-6PGL, Pgl's substrate, and γ-
227 6PGL, which forms faster by isomerization of δ-6PGL than δ-6PGL spontaneously hydrolyses to

228 6PGNT[11]. Indeed, δ-6PGL accumulation has been observed in *E. coli* BL21 growing on glucose[33]. The
229 accumulation of these reactive compounds may be detrimental to cells. The growth defect of the Δ*pgl*
230 mutant can therefore be explained by the energy cost of the Pgl bypass and/or intracellular
231 accumulation of toxic intermediates.

232 Pgl is often described as predominantly a house-cleaning enzyme, preventing the formation of
233 undesirable by-products[9,12]. According to this view, oxPPP flux should mainly be maintained by non-
234 enzymatic hydrolysis of 6PGL into 6PGNT[7,12,14]. Our results shown on the contrary that the contribution
235 of non-enzymatic δ-6PGL hydrolysis to the canonical oxPPP in the absence of Pgl is negligible, a
236 situation (absence of Pgl) that should promote non-enzymatic hydrolysis of δ-6PGL, since the
237 intracellular concentration of the latter is increased, as mentioned above[33]. We can therefore assume
238 that non-enzymatic hydrolysis of δ-6PGL is also negligible when Pgl is present (*i.e.* in the WT strain),
239 meaning that the Pgl's catalytic activity is crucial for 6PG formation. Our results therefore suggest that
240 Pgl's catalytic role is crucial for the efficient functioning of the central metabolic network. While Pgl
241 does also help prevent intracellular accumulation of 6PGLs, our results suggest that this role is
242 mediated by an additional process involving the excretion of these compounds from the cell.

243 In summary, our comprehensive functional analysis of a knock-out mutant in *E. coli*'s central
244 metabolism confirms the existence of a long described compensatory mechanisms and reveals
245 fundamental gaps in our current understanding of an enzyme operating in parallel to a non-enzymatic
246 reaction. Because the reaction catalysed by Pgl can occur spontaneously, the role of Pgl in metabolism
247 has remained unclear. Our results indicate that Pgl's catalysis of 6PGL hydrolysis into 6PGNT is crucial
248 to maintain the required flux through the oxPPP in an energy-efficient manner.

249

250 **METHODS**

251 **Strains and media.**

252 *Escherichia coli* BW25113 K-12 was selected as the experimental model (wild-type strain) for this study.
253 *E. coli* BW25113 *Δpgl* was constructed from a Δ*pgl* strain in the Keio collection[36], with kanamycin
254 cassette removal with a pCP20 plasmid encoding FLP recombinase[37]. The deletion mutant *ΔpglΔgnt*
255 was obtained via a one-step disruption protocol[38], and the triple deletion mutant *ΔpglΔgntΔIdnK*
256 similarly from the double *ΔpglΔgnt* mutant. To confirm the mutations, polymerase chain reaction (PCR)
257 was used to amplify fragments containing the modified sequences. The lengths of the amplified
258 fragments were tested by agarose gel electrophoresis and compared with those of the previous
259 mutant strain. The complemented strain (*Δpgl::pgl*) was obtained by transformation of the *Δpg*l strain
260 by a pZA23::*pgl* plasmid carrying the *pgl* gene under the control of the pLac promoter. The *pgl* gene
261 was amplified from the *E. coli* BW25113 WT strain by PCR and inserted in pZA23 plasmid using the In-
262 Fusion® HD Cloning Plus CE Kit (Takara).

263 All *E. coli* strains were grown in M9-based minimal synthetic medium as described in[6], complemented
264 with 15 mM glucose. Cultures (50 mL) were performed in triplicate in baffled shake flasks at 37 °C and
265 200 rpm. Growth was monitored by measuring the optical density at 600 nm ($OD_{600}$) using a Genesys
266 6 spectrophotometer (Thermo, USA), and a correlation factor of 0.37 ($g_{CDW}\cdot L^{-1})\cdot OD_{600}^{-1}$ was used to
267 calculate biomass concentration.

268 **NMR analysis**

269 NMR spectra were recorded on a Bruker Avance III HD 800 MHz spectrometer equipped with a 5-mm
270 quadruple-resonance QCI-P (H/P-C/N/D) cryogenically cooled probe head. $D_2O$ (10 vol.%) was added
271 to the samples for field/frequency locking and 1 mM TSP-d4 (dissolved in $D_2O$) was added as an internal
272 standard for frequency calibration and concentration measurements. Spectra were recorded and
273 processed using Bruker TopSpin 3.2. 1D $^1$H NMR spectra were acquired using the zgpr30 sequence at
274 280 K with 32 or 64 scans, 64k points, an acquisition time of 2 s, and an recycle delay of 8 s.

275 **Extracellular metabolite concentration measurements and calculation of extracellular fluxes.**

276 Metabolite concentrations (glucose, acetate, gluconate (GNT)) were quantified by 1D$^{1}$H NMR from the
277 supernatant obtained by centrifugation (12,000 g, 3 min) of culture broth. The 1D $^{1}$H NMR data were
278 acquired as described above (64 scans). For samples containing gluconolactone (GL), the metabolites
279 (including glucose, gluconate and gluconolactone) were quantified immediately after filtration (0.2
280 µm, polyethersulfone membrane) of 500 µL of culture. The filtrate was kept on ice and rapidly analysed
281 by NMR as described above (32 scans).

282 Extracellular fluxes (*i.e.* glucose uptake, GNT accumulation and growth rates) were determined from
283 the time course concentrations of biomass, substrates, and products using PhysioFit
284 v2.0.4[39](https://github.com/MetaSys-LISBP/PhysioFit).

285 **Stationary $^{13}$C- labelling experiments**

286 After preculture on LB, strains were grown in 50 ml M9 minimal synthetic medium complemented with
287 15 mM [1-$^{13}$C] glucose in baffled shake flasks at 37 °C and 200 rpm. At OD 1.2, cells were harvested by
288 centrifugation (5 min at 10,000 g) and the pellet was resuspended in 1.250 ml of Milli-Q $H_2O$. The
289 suspension (250 µl) was mixed with 250 µl of HCl 12N and hydrolysed at 110 °C for 18 h. HCl was
290 evaporated using a vacuum concentrator, the pellet was washed twice with Milli-Q $H_2O$ and
291 resuspended in 100 µl $H_20$. This sample was diluted 100 times for analysis. The carbon isotopologue
292 distribution of alanine was measured in three independent biological replicates, as detailed in[40].

293 **$^{13}$C-Pulse experiments**

294 *E. coli* BW25113 *Δpgl* was grown in 50 ml M9 minimal synthetic medium complemented with 15 mM
295 glucose in a baffled shake flask at 37 °C and 200 rpm. At OD 1.2, [2-$^{13}$C] glucose was added to the
296 culture medium to obtain approximately 50 % of $^{13}$C-labelled glucose. Growth was monitored using
297 $OD_{600}$ measurements as described above. Extracellular compounds were quantified directly by NMR as
298 described above.

299 **Kinetics of phosphogluconolactone and gluconolactone spontaneous hydrolysis**

300 *Real time monitoring of gluconolactone (GL) degradation*. δ-Gluconolactone (δ-GL) degradation was
301 monitored by $^{1}$H NMR using a pseudo-2D pulse program (noesyphpr) at 310K. A 3 mM δ-GL (Sigma-
302 Aldrich) solution was prepared in M9-based minimal synthetic medium. Acquisitions were started after
303 rapid homogenisation and temperature stabilisation, and spectra were recorded every 65 s with 8
304 scans each (acquisition time, 3 s; recycle delay, 5 s) for a total of 120 time points. δ-GL degradation at
305 280 K was monitored using the same procedure and a freshly prepared δ-GL solution.

306 *Real time monitoring of 6-phosphogluconolactone (6PGL) degradation*. 6PGL was produced
307 enzymatically from glucose-6-phosphate (G6P) using commercial *L. mesenteroides* $NADP^{+}$ dependent
308 G6P-dehydrogenase (G6PDH) expressed in *E. coli* (Sigma-Aldrich). The reaction mix consisted of 5 mM
309 G6P, 5 mM $NADP^{+}$, 12 mM $MgCl_2$, 100 mM phosphate buffer (at pH = 7.2) and 1 mM TSP-d4[6]. $^{1}$H and
310 $^{31}$P 1D NMR spectra of the mix were recorded using the zgpr30 sequence with 16 scans and the zg
311 sequence with 64 scans, respectively. One enzyme unit of G6PDH was then added to the NMR tube
312 and the production and hydrolysis of 6PGL were monitored at 310 K using dual reception ($^{1}$H and $^{31}$P)
313 pseudo-2D spectra (2DDR zggpw5)[41]. Spectra were recorded every 115 s with 64 scans each for a total
314 of 64 time points ($^{1}$H acquisition time, 0.7 s; recycle delay; $^{31}$P acquisition time 0.6 s, recycle delay, 1
315 s). The concentrations of G6P, 6PGL and 6PGNT were determined from the rows of the pseudo-2D $^{31}$P
316 spectra.

317 *Calculation of degradation constants***.** The degradation constants of GL and 6PGL were determined by
318 fitting their time-course concentrations assuming a first-order process using COPASI[42] (v4.27), as
319 detailed in[17].

320 **Relative contributions of glycolysis and the oxPPP**

321 The contributions of the oxPPP and Emben-Meyerhof-Parnas (EMP) pathway to glucose metabolism
322 were estimated by quantifying alanine isotopologues. [1-$^{13}$C] glucose metabolised through the EMP
323 pathway forms unlabelled and [1-$^{13}$C] pyruvate in equal proportions, while $C_1$-decarboxylation of

324 glucose through the oxPPP only produces unlabelled pyruvate. The contributions of the oxPPP and the
325 EMP pathway were thus estimated from the fraction of the M1 isotopologue of alanine, using the
326 following algebraic equations[21]:

327 $$Glycolysis = 2 \times Ala_{M1}$$

328 $$PPP = 2 \times (0.5 - Ala_{M1})$$

329

330 **Dynamic $^{13}$C-flux model of glucose metabolism to quantify the contribution of the Pgl bypass**

331 To quantify the contributions of the canonical oxPPP and of the Pgl bypass to ribose-5-phosphate
332 biosynthesis, we constructed a dynamic $^{13}$C-flux model of glucose metabolism following the formalism
333 detailed in[43]. The model contains 21 reactions, 25 species, and 2 compartments (the environment and
334 the cell), and represents five processes: i) growth, ii) glucose uptake and phosphorylation into G6P,
335 utilisation of G6P through iii) the EMP pathway and iv) the intracellular branch of the oxPPP, and v) the
336 extracellular Pgl bypass (Figure 4).

337 The differential equations, which balance the concentrations of extracellular compounds (biomass,
338 glucose, gluconolactone and gluconate) and intracellular compounds (G6P, glyceraldehyde-3-
339 phosphate, 6PGL, 6PGNT and pyruvate), were completed with isotopic equations for parameter
340 estimation. As detailed in [43,44], we considered all reactions (except biomass synthesis) separately for
341 unlabelled and labelled reactants. Fluxes were assumed to be constant over time, in line with the
342 metabolic steady-state assumption, except for the gluconolactone hydrolysis flux which was modelled
343 using the mass action law to represent first-order degradation kinetics[17], in keeping with the abiotic
344 hydrolysis of gluconolactone into gluconate (see Results).

345 The final model has 8 free parameters in total (Supplementary 2). The contribution of the oxPPP to
346 glucose metabolism (*i.e.* the sum of the flux through the intra- and extracellular branches of the oxPPP)
347 and the gluconolactone (abiotic) hydrolysis rate were fixed at the experimental values determined in
348 this study, as detailed in the Results section. The remaining parameters (p) were estimated by fitting

349 to the experimentally determined concentration dynamics of biomass and unlabelled and labelled
350 glucose and gluconolactone, by minimising the objective function $f$ defined as the weighted sum of
351 squared errors:

352 $$f(p) = \sum_i \left(\frac{x_i - y_i(p)}{\sigma_i}\right)^2$$

353 where $x_i$ is the experimental value of data point $i$, with an experimental standard deviation $\sigma_i$, and $y_i(p)$
354 is the corresponding simulated value. The objective function $f$ was minimised using the particle swarm
355 optimisation algorithm (2,000 iterations with a swarm size of 50). The experimental and fitted data of
356 one biological replicate are shown in Figure 4, and the data for all replicates are provided in the
357 Supplementary 2.

358 The model was constructed and analysed using COPASI[42] (v4.27) and is provided in SBML and COPASI
359 formats in the Supplementary 2 and at https://github.com/MetaSys-LISBP/GL_GNT_bypass. The
360 model has also been deposited in the Biomodels database (https://www.ebi.ac.uk/biomodels)[45] with
361 the identifier MODEL2310250001 to ensure reproducibility and reusability.

362 **Supplementary Material**

363 Supplementary material 1 : Figure 1, Figure 2, figure 3 et Figure 4

364 Supplementary material 2: Model documentation

365 **Acknowledgements**

366 This study was funded by the Agence Nationale de la Recherche, grant number ANR-19-CE44-0005
367 (PerioMet).

368 The authors thank MetaToul (Metabolomics & Fluxomics Facilities, Toulouse, France,
369 www.metatoul.fr) and its staff for technical support and access to the NMR facility. MetaToul is part
370 of the French National Infrastructure for Metabolomics and Fluxomics (www.metabohub.fr), funded
371 by the ANR (MetaboHUB-ANR-11-INBS-0010).

373 **REFERENCES**


374 1. Edwards, J. S. & Palsson, B. O. Robustness analysis of the Escherichia coli metabolic network.
375 *Biotechnol Prog* 16, 927–939 (2000).
376 2. Nakahigashi, K. *et al.* Systematic phenome analysis of Escherichia coli multiple-knockout mutants
377 reveals hidden reactions in central carbon metabolism. *Mol Syst Biol* 5, 306 (2009).
378 3. Emmerling, M. *et al.* Metabolic flux responses to pyruvate kinase knockout in Escherichia coli. *J*
379 *Bacteriol* 184, 152–164 (2002).
380 4. Jiao, Z., Baba, T., Mori, H. & Shimizu, K. Analysis of metabolic and physiological responses to gnd
381 knockout in Escherichia coli by using C-13 tracer experiment and enzyme activity measurement.
382 *FEMS Microbiol Lett* 220, 295–301 (2003).
383 5. Siddiquee, K. A. Z., Arauzo-Bravo, M. J. & Shimizu, K. Effect of a pyruvate kinase (pykF-gene)
384 knockout mutation on the control of gene expression and metabolic fluxes in Escherichia coli.
385 *FEMS Microbiology Letters* 235, 25–33 (2004).
386 6. Nicolas, C. *et al.* Response of the central metabolism of Escherichia coli to modified expression of
387 the gene encoding the glucose-6-phosphate dehydrogenase. *FEBS Lett.* 581, 3771–3776 (2007).
388 7. Long, C. P. & Antoniewicz, M. R. Metabolic flux responses to deletion of 20 core enzymes reveal
389 flexibility and limits of E. coli metabolism. *Metabolic Engineering* 55, 249–257 (2019).
390 8. Sorokina, M., Stam, M., Médigue, C., Lespinet, O. & Vallenet, D. Profiling the orphan enzymes.
391 *Biology Direct* 9, 10 (2014).
392 9. Keller, M. A., Piedrafita, G. & Ralser, M. The widespread role of non-enzymatic reactions in cellular
393 metabolism. *Current Opinion in Biotechnology* 34, 153–161 (2015).
394 10. Rakitzis, E. T. & Papandreou, P. Reactivity of 6-phosphogluconolactone with hydroxylamine: The
395 possible involvement of glucose-6-phosphate dehydrogenase in endogenous glycation reactions.
396 *Chemico-Biological Interactions* 113, 205–216 (1998).
397 11. Miclet, E. *et al.* NMR spectroscopic analysis of the first two steps of the pentose-phosphate
398 pathway elucidates the role of 6-phosphogluconolactonase. *J Biol Chem* 276, 34840–34846 (2001).

399 12. Galperin, M. Y., Moroz, O. V., Wilson, K. S. & Murzin, A. G. House cleaning, a part of good
400 housekeeping. *Molecular Microbiology* 59, 5–19 (2006).
401 13. Kupor, S. R. & Fraenkel, D. G. 6-phosphogluconolactonase mutants of Escherichia coli and a
402 maltose blue gene. *J Bacteriol* 100, 1296–1301 (1969).
403 14. Kupor, S. R. & Fraenkel, D. G. Glucose Metabolism in 6-Phosphogluconolactonase Mutants of
404 Escherichia coli. *Journal of Biological Chemistry* 247, 1904–1910 (1972).
405 15. Thomason, L. C., Court, D. L., Datta, A. R., Khanna, R. & Rosner, J. L. Identification of the Escherichia
406 coli K-12 ybhE gene as pgl, encoding 6-phosphogluconolactonase. *J Bacteriol* 186, 8248–8253
407 (2004).
408 16. Enjalbert, B., Letisse, F. & Portais, J.-C. Physiological and Molecular Timing of the Glucose to
409 Acetate Transition in Escherichia coli. *Metabolites* 3, 820–837 (2013).
410 17. Peiro, C. *et al.* Chemical and Metabolic Controls on Dihydroxyacetone Metabolism Lead to
411 Suboptimal Growth of Escherichia coli. *Appl Environ Microbiol* 85, (2019).
412 18. Tong, S., Porco, A., Isturiz, T. & Conway, T. Cloning and molecular genetic characterization of the
413 Escherichia coli gntR, gntK, and gntU genes of GntI, the main system for gluconate metabolism.
414 *Journal of Bacteriology* 178, 3260–3269 (1996).
415 19. Istúriz, T., Palmero, E. & Vitelli-Flores, J. Mutations affecting gluconate catabolism in Escherichia
416 coli. Genetic mapping of the locus for the thermosensitive gluconokinase. *J Gen Microbiol* 132,
417 3209–3219 (1986).
418 20. Bausch, C., Ramsey, M. & Conway, T. Transcriptional Organization and Regulation of the l-Idonic
419 Acid Pathway (GntII System) in Escherichia coli. *Journal of Bacteriology* 186, 1388–1397 (2004).
420 21. Millard, P., Cahoreau, E., Heuillet, M., Portais, J.-C. & Lippens, G. 15N-NMR-Based Approach for
421 Amino Acids-Based 13C-Metabolic Flux Analysis of Metabolism. *Anal. Chem.* 89, 2101–2106
422 (2017).
423 22. Neidhart, F. C. & Curtiss, R. Escherichia coli and Salmonella—Cellular and molecular biology. in
424 *Escherichia coli and Salmonella—Cellular and molecular biology* (SM Press, 1996).

425 23. Reaves, M. L., Young, B. D., Hosios, A. M., Xu, Y.-F. & Rabinowitz, J. D. Pyrimidine homeostasis is
426 accomplished by directed overflow metabolism. *Nature* 500, 237–241 (2013).
427 24. Aon, J. C. *et al.* Suppressing Posttranslational Gluconoylation of Heterologous Proteins by
428 Metabolic Engineering of *Escherichia coli*. *Appl Environ Microbiol* 74, 950–958 (2008).
429 25. Chang, D.-E. *et al.* Carbon nutrition of Escherichia coli in the mouse intestine. *Proc Natl Acad Sci U*
430 *S A* 101, 7427–7432 (2004).
431 26. Neidhart, F. C., Ingraham, J. L. & Schaechter, M. *Physiology of the bacterial cell: a molecular*
432 *approach.* (1990).
433 27. Robin, A. & Kepes, A. The mechanism of maintenance of electroneutrality during the transport of
434 gluconate by E. coli. *FEBS Letters* 36, 133–136 (1973).
435 28. Steigmiller, S., Turina, P. & Gräber, P. The thermodynamic H+/ATP ratios of the H+-ATPsynthases
436 from chloroplasts and Escherichia coli. *Proc Natl Acad Sci U S A* 105, 3745–3750 (2008).
437 29. Ishii, N. *et al.* Multiple High-Throughput Analyses Monitor the Response of E. coli to Perturbations.
438 *Science* 316, 593–597 (2007).
439 30. Theodosiou, E., Frick, O., Bühler, B. & Schmid, A. Metabolic network capacity of Escherichia coli for
440 Krebs cycle-dependent proline hydroxylation. *Microbial Cell Factories* 14, 108 (2015).
441 31. Kim, H., Kim, S. & Yoon, S. H. Metabolic network reconstruction and phenome analysis of the
442 industrial microbe, Escherichia coli BL21(DE3). *PLOS ONE* 13, e0204375 (2018).
443 32. Terpe, K. Overview of bacterial expression systems for heterologous protein production: from
444 molecular and biochemical fundamentals to commercial systems. *Appl Microbiol Biotechnol* 72,
445 211–222 (2006).
446 33. Meier, S., Jensen, P. R. & Duus, J. Ø. Direct observation of metabolic differences in living
447 Escherichia coli strains K-12 and BL21. *Chembiochem* 13, 308–310 (2012).
448 34. Fischer, E. & Sauer, U. Metabolic flux profiling of Escherichia coli mutants in central carbon
449 metabolism using GC-MS. *European Journal of Biochemistry* 270, 880–891 (2003).

450 35. Zhao, J., Baba, T., Mori, H. & Shimizu, K. Effect of zwf gene knockout on the metabolism of
451 Escherichia coli grown on glucose or acetate. *Metab Eng* 6, 164–174 (2004).
452 36. Baba, T. *et al.* Construction of Escherichia coli K-12 in-frame, single-gene knockout mutants: the
453 Keio collection. *Mol. Syst. Biol.* 2, 2006.0008 (2006).
454 37. Cherepanov, P. P. & Wackernagel, W. Gene disruption in Escherichia coli: TcR and KmR cassettes
455 with the option of Flp-catalyzed excision of the antibiotic-resistance determinant. *Gene* 158, 9–14
456 (1995).
457 38. Datsenko, K. A. & Wanner, B. L. One-step inactivation of chromosomal genes in Escherichia coli K-
458 12 using PCR products. *Proc Natl Acad Sci U S A* 97, 6640–6645 (2000).
459 39. Grégam, L. L. *et al.* PhysioFit: a software to quantify cell growth parameters and extracellular
460 fluxes. 2023.10.12.561695 Preprint at https://doi.org/10.1101/2023.10.12.561695 (2023).
461 40. Heuillet, M. *et al.* Methodology for the Validation of Isotopic Analyses by Mass Spectrometry in
462 Stable-Isotope Labeling Experiments. *Anal. Chem.* 90, 1852–1860 (2018).
463 41. Cox, N. *et al.* Integrated pH Measurement during Reaction Monitoring with Dual-Reception 1H-
464 31P NMR Spectroscopy. *Anal Chem* 91, 3959–3963 (2019).
465 42. Hoops, S. *et al.* COPASI--a COmplex PAthway SImulator. *Bioinformatics* 22, 3067–3074 (2006).
466 43. Millard, P., Portais, J.-C. & Mendes, P. Impact of kinetic isotope effects in isotopic studies of
467 metabolic systems. *BMC Syst Biol* 9, 64 (2015).
468 44. Enjalbert, B., Millard, P., Dinclaux, M., Portais, J.-C. & Létisse, F. Acetate fluxes in Escherichia coli
469 are determined by the thermodynamic control of the Pta-AckA pathway. *Sci Rep* 7, 42135 (2017).
470 45. Chelliah, V. *et al.* BioModels: ten-year anniversary. *Nucleic Acids Res* 43, D542-548 (2015).
471 46. Le Novère, N. *et al.* The Systems Biology Graphical Notation. *Nat Biotechnol* 27, 735–741 (2009).
472

473

474 **TABLES**

475 **Table 1: Growth parameters of the different *E. coli* BW25113 strains grown in minimal media with**
476 **15mM glucose.**

477 The growth of the *E. coli* BW25113 *Δpgl* strain was compared to the WT strain's and that of the
478 complemented strain, Δ*pgl*::pZA23*pgl*, obtained by transformation of the *Δpgl* strain with pZA23::pgl
479 plasmid and of the Δ*pgl*::pZA23 strain with an empty plasmid. $\mu_{max}$, growth rate; $q_{Glc}$, specific glucose
480 uptake rate; $q_{Ac}$, specific net acetate production rate; $q_{Gnt}$, specific gluconate accumulation rate.
481 Results are the mean ± SD of three biologically independent samples.

| Parameters | WT | Δ*pgl* | Δ*pgl*::pZA23*pgl* | Δ*pgl*::pZA23 |
|---|---|---|---|---|
| $\mu_{max}$ ($h^{-1}$) | 0.61 ± 0.01 | 0.43 ± 0.01 | 0.57 ± 0.01 | 0.41 ± 0.01 |
| $q_{Glc}$ (mmol · [$g_{CDW}$ · h]$^{-1}$) | 7.77 ± 0.17 | 8.52 ± 0.39 | 10.11 ± 0.83 | 7.60 ± 0.08 |
| $q_{Ace}$ (mmol · [$g_{CDW}$ · h]$^{-1}$) | 2.37 ± 0.15 | 4.56 ± 0.16 | 7.60 ± 0.31 | 3.95 ± 0.16 |
| $q_{Gnt}$ (mmol · [$g_{CDW}$ · h]$^{-1}$) | 0 | 0.17 ± 0.01 | 0 | 0.14 ± 0.02 |

482

483

484

485

486 **FIGURES**

487

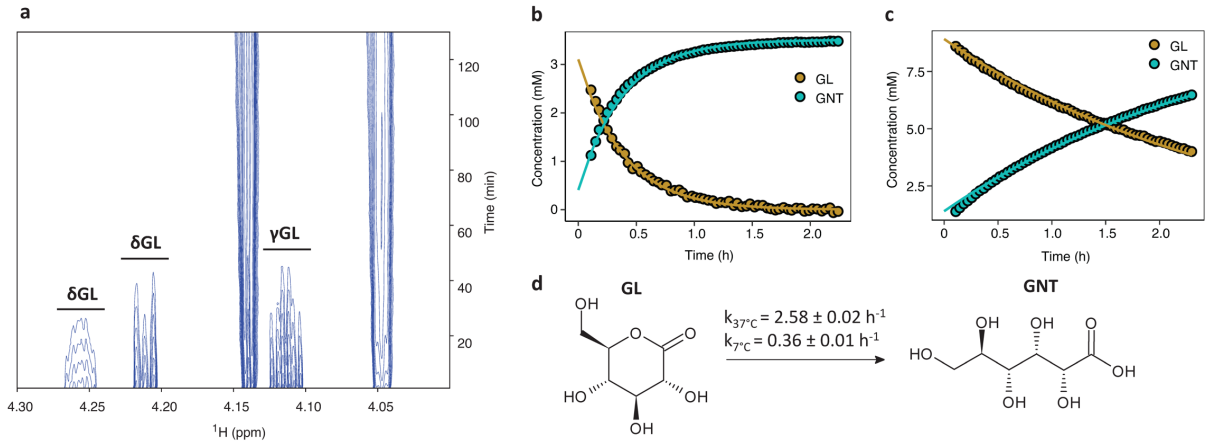


488 **Figure 1. Gluconolactone spontaneous hydrolysis**. **a**. Pseudo-2D $^1$H spectra at 37°C, pH7.2 in M9
489 synthetic minimal media of spontaneous gluconolactone hydrolysis. T0 corresponds to the beginning
490 of NMR acquisition (= 6 min 35 s after gluconolactone addition). **b,c**. GL and GNT concentrations
491 extracted from pseudo-2D spectra (dots) and fitted by COPASI model (lines) at 37 °C (**b**) and 7 °C (**c**). **d.**
492 Reaction scheme for the spontaneous hydrolysis of gluconolactone (GL) into gluconic acid (GNT) with
493 the degradation constant obtained at 37 °C and 7 °C.

494

495

496 **Figure 2:**

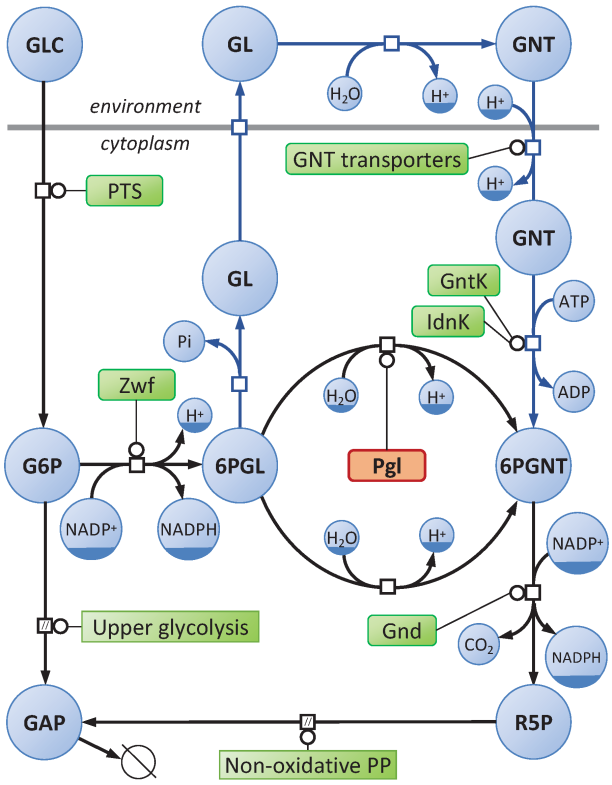


497

498 **Figure 2. Schematic representation of the Pgl bypass and of the oxidative branch of the pentose-**
499 **phosphate (PP) pathway in *E. coli*, in Systems Biology Graphical Notation format**[46]
500 **(http://sbgn.org.io).** Circles represent metabolites and rounded rectangles represent enzymes. GLC,
501 glucose; G6P, glucose-6-phosphate; GAP, glyceraldehyde-3-phosphate; 6PGL, 6-
502 phosphogluconolactone; GL, gluconolactone; GNT, gluconate; 6PGNT, 6-phosphogluconate; R5P,
503 ribulose-5-phosphate; PTS, Phosphoenolpyruvate:glucose phosphotransferase system; Zwf, glucose-
504 6-phosphate dehydrogenase; GntK, gluconate kinase; IdnK, thermosensitive gluconate kinase; Gnd, 6-
505 phosphogluconate.

506

507 **Figure 3**

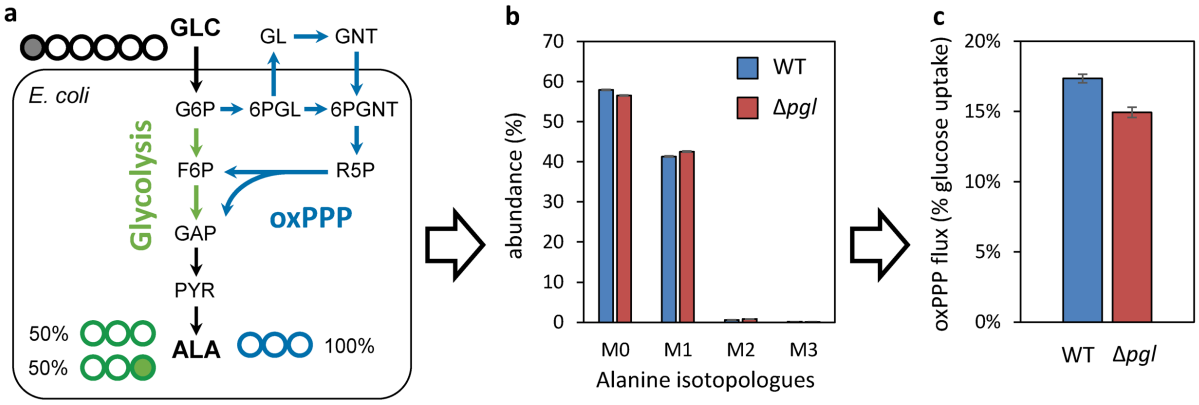


508

509 **Figure 3. Metabolic fluxes analysis of *E. coli* BW25113 wild-type (WT) and Δ*pgl* strains.**

510 **a**. Cells were grown on 1-$^{13}$C-glucose, which can be metabolized through glycolysis (green pathway)

511 and the pentose phosphate pathway (blue pathway). Filled (empty) circles represent $^{13}$C ($^{12}$C) atoms.

512 **b**. Isotopologue distribution of alanine measured by mass spectrometry. **c**. The partitioning of carbon

513 fluxes between glycolysis and the pentose phosphate pathway was quantified from the data shown in

514 panel b. The bars represent the mean of three biological replicates, and the error bars represent one

515 standard deviation.

516

517 **Figure 4 :**

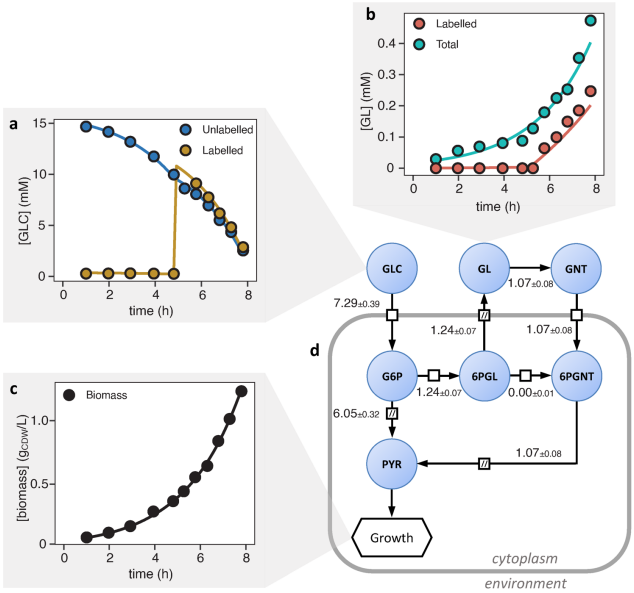


518

519 **Figure 4. Fluxes in the oxPPP of *E. coli* BW25113 Δ*pgl* quantified by non-stationary $^{13}$C-metabolic flux**

520 **analysis.**

521 **a.** Concentrations of labelled and unlabelled glucose. [2-$^{13}$C]-glucose was added at mid-exponential

522 growth (approx. 5 h). **b.** Gluconolactone (labelled and total) concentrations. **c.** Growth of the Δ*pgl*

523 strain as a function of time. **d.** Metabolic network of the model used to calculate fluxes involved in the

524 Pgl bypass, with flux results (obtained from three independent biological replicates).

525

526